Available online at www.sciencedirect.com
SCIENCE DIRECT
Earth and Planetary Science Letters 241 (2006) 876–887
EPSL
www.elsevier.com/locate/epsl

Active and buried authigenic barite fronts in sediments from the Eastern Cape Basin

N. Riedinger [a,*], S. Kasten [a,1], J. Gröger [a], C. Franke [a,b], K. Pfeifer [a]

[a] Fachbereich Geowissenschaften, Universität Bremen, Klagenfurter Straße, 28359 Bremen, Germany
[b] Paleomagnetic Laboratory, Fort Hoofddijk', Utrecht University, Budapestlaan 17, 3584 CD Utrecht, The Netherlands

Received 15 April 2005; received in revised form 19 October 2005; accepted 27 October 2005
Available online 15 December 2005
Editor: H. Elderfield

Abstract

Sediment cores retrieved in the Benguela coastal upwelling system off Namibia show very distinct enrichments of solid phase barium at the sulfate/methane transition (SMT). These barium peaks represent diagenetic barite ($BaSO_4$) fronts which form by the reaction of upwardly diffusing barium with interstitial sulfate. Calculated times needed to produce these barium enrichments indicate a formation time of about 14,000 yr. Barium spikes a few meters below the SMT were observed at one of the investigated sites (GeoB 8455). Although this sulfate-depleted zone is undersaturated with respect to barite, the dominant mineral phase of these buried barium enrichments was identified as barite by scanning electron microscopy (SEM). This is the first study which reports the occurrence/preservation of pronounced barite enrichments in sulfate-depleted sediments buried a few meters below the SMT. At site GeoB 8455 high concentrations of dissolved barium in pore water as well as barium in the solid phase were observed. Modeling the measured barium concentrations at site GeoB 8455 applying the numerical model CoTReM reveals that the dissolution rate of barite directly below the SMT is about one order of magnitude higher than at the barium enrichments deeper in the sediment core. This indicates that the dissolution of barite at these deeper buried fronts must be retarded. Thus, the occurrence of the enrichments in solid phase barium at site GeoB 8455 could be explained by decreased dissolution rates of barite due to the changes in the concentration of barite in the sediment, as well as changes in the saturation state of fluids. Furthermore, the alteration of barite into witherite ($BaCO_3$) via the transient phase barium sulfide could lead to the preservation of a former barite front as $BaCO_3$. The calculations and modeling indicate that a relocation of the barite front to a shallower depth occurred between the last glacial maxium (LGM) and the Pleistocene/Holocene transition. We suggest that an upward shift of the SMT occurred at that time, most likely as a result of an increase in the methanogenesis rates due to the burial of high amounts of organic matter below the SMT.

Keywords: authigenic barite; Benguela upwelling system; anaerobic oxidation of methane (AOM); non-steady state diagenesis; whiterite ($BaCO_3$)

1. Introduction

Sediments which underlay areas of high primary productivity are often enriched in barium bearing solid phases [1–5]. The link between productivity and the amount of barium in the sediment is thought to be established by the formation of distinct barite ($BaSO_4$)

* Corresponding author. Current address: Max-Planck-Institute for Marine Microbiology, Celsiusstrasse 1, 28359 Bremen, Germany. Tel.: +49 421 2028 634; fax: +49 421 2028 690.
E-mail address: nar@uni-bremen.de (N. Riedinger).
[1] Current address: Alfred Wegener Institute for Polar and Marine Research, Am Handelshafen 12, 27570 Bremerhaven, Germany.

0012-821X/$ - see front matter © 2005 Elsevier B.V. All rights reserved.
doi:10.1016/j.epsl.2005.10.032

particles in the water column associated with the decay of organic matter or rather the decay of phytoplankton [3,6–8]. Thus, in marine deposits barite is often used as a tracer of paleoproductivity [9–12]. Besides the utilization of excess barium, in particular barite, as a productivity-proxy several other indications can be drawn from barium compounds. Marine barite is often used to reconstruct past Sr isotope compositions of seawater, or for Sr isotope stratigraphy [13,14]. Furthermore it can be applied to reconstruct the former sulfur isotope ratio of marine sulfate [15,16], or to draw conclusions about past changes in the upward flux of methane [17].

However, the use of barium as a proxy (e.g. for paleoproductivity) is clearly limited as shown in several studies [9,12,18]. The alteration of the primary barium signal by diagenetic processes is one of the most important limitations for the application of barium and barium-compounds as a proxy. Generally, barite is relatively resistant to alteration after burial [14,19]. However, in zones of sulfate depletion barite is dissolved and barium is released into the pore water. The upward transport of barium by diffusion into sulfate-bearing pore waters is leading to precipitation of authigenic barite in diagenetic fronts. Thus, barite fronts are mainly found directly above the sulfate penetration depth, at the sulfate/methane transition (SMT) [9,17,20–22]. The formation of authigenic barite fronts is affected by diagenetic alteration due to sulfate reduction and driven by anaerobic oxidation of methane (AOM) [17,23]. Nonsteady-state diagenesis greatly influences authigenic barite precipitation [24]. Drastic decreases in sedimentation rate can fix the barite front at a discrete interval which can lead to the formation of large barite deposits [22]. Moreover, changes in methane flux can shift the SMT and thus the position of the barite front [17]. Thus, barite fronts can be used to reconstruct changes in the upward flux of methane. However, generally only former barite fronts above the current depth of the SMT which formed in association with a downward migration of the SMT can be used. Burial of barite enrichments in sulfate-depleted sediments is assumed to result in their fast dissolution. Up to now, barium enrichments preserved below the SMT have only been described in deeply buried sediments, drilled by the ODP (Ocean Drilling Program). These barium enrichments were mostly described as the result of hydrothermal intrusions or associated with fluid seeps [9,25,26].

In this study we report on barite enrichments at the SMT and in addition we present data of solid phase Ba-enrichments in the sulfate-depleted zone. Scanning electron microscopy (SEM) and energy dispersive spectrometry (EDS) were carried out for identification and semi-quantification of the Ba phases in the sediment. Furthermore, we discuss the mechanisms and/or conditions which lead to the preservation of the barite enrichments below the SMT. To investigate the processes involved, we applied numerical modeling of the geochemical data and we calculated the time needed to produce the barium peaks observed.

2. Materials and methods

2.1. Sampling sites

The gravity cores (Table 1) investigated in this study were retrieved on a down slope transect (T2) on the continental margin off Namibia in the eastern South Atlantic (Fig. 1) during RV *Meteor* expeditions M34/2 and M57/2. The sediments in the Eastern Cape Basin are characterized by low input of terrigenous matter and high biogenic contents. The high amounts of organic matter (up to 12 wt.% at site GeoB 8426, and 9 wt.% at site GeoB 8455) in the sediment are due to the enhanced primary productivity in the surface water [10,27]. The Benguela upwelling system is controlled by the predominant southeasterly trade-winds that drive the coastal upwelling of cold and nutrient-rich water [28,29]. Occasional berg winds, perpendicular to the coast, are the most important means of transport for terrestrial material [29,30]. Minor amounts of terrigenous sediment are supplied by perennial rivers (Orange River) and rivers sporadically carrying water, like the Swakop River [31]. The deposition of river discharge is limited to the shelf, and the slope mainly consists of calcareous ooze [31,32]. Quaternary slumps and slides can only be found close to the Walvis Ridge [27,33] and do not represent important sediment transport processes in the study area.

2.2. Sampling and sample processing

The sampling procedures and analytical techniques are only briefly described below. For detailed infor-

Table 1
Location and water depth of GeoB stations of the investigated gravity cores

Stations	Longitude [E]	Latitude [S]	Water depth [m]
GeoB 3703-8	13°13.8	25°31.1	1369
GeoB 3718-9	13°09.8	24°53.6	1312
GeoB 8426-3	13°21.1	25°28.9	1045
GeoB 8455-2	13°11.0	25°30.4	1503

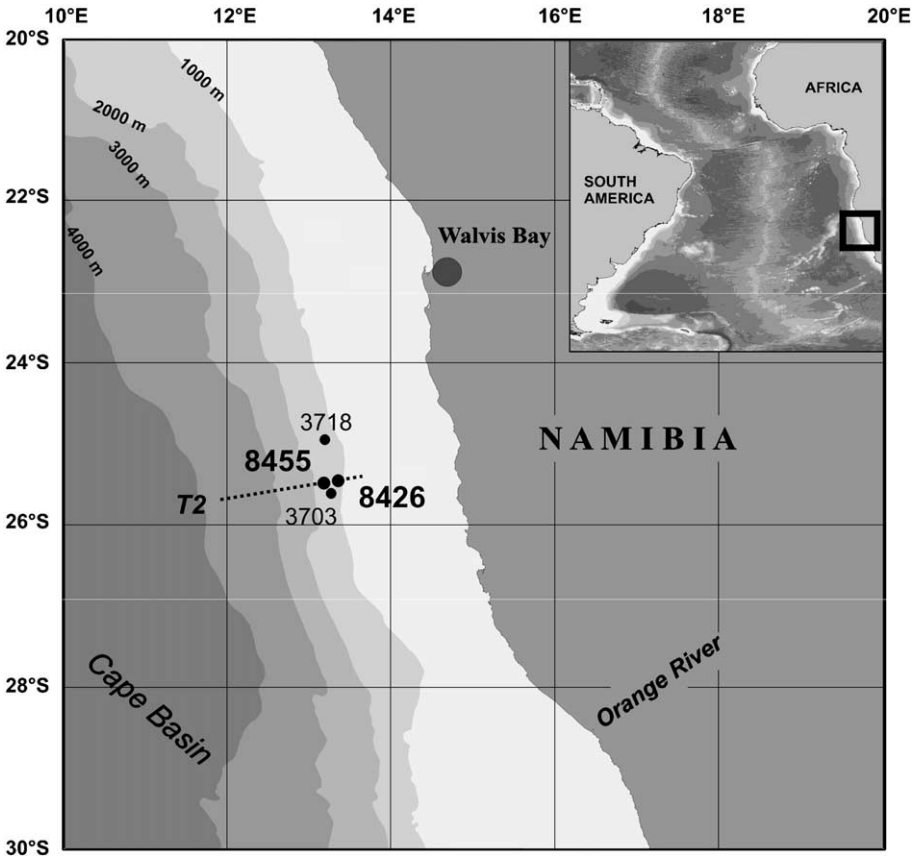

Fig. 1. Map displaying the location of the investigated gravity cores taken at the GeoB stations. The dotted line marks the transect 2 (T2).

mation regarding analytical methods and devices, the reader is referred to Schulz [34] and to the homepage of the geochemistry group http://www.geochemie.uni-bremen.de at the University of Bremen. The set of pore water and solid phase data is available via the geological data network Pangaea (http://www.pangaea.de/PangaVista?query=@Ref26531).

Immediately after retrieval gravity cores were cut into 1 m segments on deck and from the bottom of every segment syringe samples were taken for methane analysis. Syringe samples of 5 mL of sediment were injected into 50 mL septum vials containing 20 mL of seawater, and were stored at −20 °C. To prevent warming of the sediments, all cores were placed in a cooling container and were maintained at a temperature of about 4 °C. Within the first 2 days after recovery, gravity cores were cut lengthwise into two halves and were processed in a glove box under argon atmosphere. Sediment samples were taken every 25 cm for pressure filtration. Solid phase samples for total digestions, sequential extractions and mineralogical analyses were taken at 10 cm intervals and were kept in gas-tight glass bottles under argon atmosphere. To suppress subsequent alteration processes the storage temperature for all sediments was −20 °C. Teflon-squeezers fitted with 0.2 μm cellulose acetate membrane filters were used for pressure filtration (5 bar). For H_2S determination, 1 mL sub samples of the pore water were added to a ZnAc-solution (400 μL) in order to fix all sulfide as ZnS. Sub samples for sulfate determination were diluted 1:20 and stored frozen for ion chromatography (HPLC). All further analyses were carried out at the University of Bremen. Methane was measured with a gas chromatograph (*Varian 3400*) equipped with a splitless injector, by injecting 20 μL of the headspace gas. The concentrations were subsequently corrected for sediment porosity. H_2S was determined using a titration method. Aliquots of the remaining pore water were diluted, and acidified with HNO_3 for determination of cations by atomic absorption spectrometry (AAS, *Unicam Solaar 989 QZ*), and inductively coupled plasma atomic emission spectrometry (ICP-AES, *Perkin Elmer Optima 3000 RL*).

All solid phase analyses were performed on anoxic sub samples. Sample solutions obtained by total acid digestion were analyzed by ICP-AES, with an analytical precision of less than 3%. Solid phase samples from site GeoB 3703 were measured using X-ray fluorescence (XRF). Approximately 4 g of freeze dried and homogenized sediment material was poured into sample cups, and analyzed using the compact benchtop energy-dispersive polarization XRF (EDP-XRF) analysis system *Spectro Xepos*. Total carbon (TC) and total organic carbon (TOC) contents were determined by measuring freeze-dried and homogenized samples using a *LECO CS-300* carbon sulfur analyzer. For organic carbon analysis, the samples were treated with 12.5% HCl, washed two times with Milli Q, and dried at 60 °C. The accuracy, checked by marble standards, was ± 3%. Sediment physical measurements of electrical resistivity, as a measure of porosity and density, were performed at a resolution of 1 cm on board using a *GEOTEK* Multi-Sensor Core Logger (MSCL). Selected dry bulk sediment samples were analyzed by scanning electron microscopy (SEM) using a *Philips XL30 SFEG* (operating between 10 and 12 kV) equipped with an *EDAX* energy dispersive spectrometer (EDS). The non-embedded powder samples were fixed on a carbon sticker, previously stuck onto the top of a standard SEM stub, and coated under argon atmosphere with a 5 nm Pt/Pd layer.

2.3. Geochemical modeling

To simulate the process of barite dissolution and reprecipitation, the column transport and reaction model CoTReM was used. A detailed description of this computer software is given in the CoTReM User Guide [35] and by Adler et al. [36]. The transport mechanism for the solid phase and pore water is the sedimentation rate. The solutes in the pore water are transported by molecular diffusion (D_s). Diffusion coefficients were corrected for tortuosity [37] and temperature (3 °C). The model area, representing the core length of 12 m, was subdivided into cells of 5 cm thickness. The time step to fulfill numerical stability was set to 1×10^{-1} yr. Zero-order kinetics are calculated for the given reaction by defining maximum reaction rates. The calculation of the reaction-specific change in concentration at a specific depth ($\Delta C_{s,d}$) is according to the equation:

$$\Delta C_{s,d} = R_{s,d} \times dt_{num} \times SC_{s,d} \quad (1)$$

Where $R_{s,d}$ [mol L^{-1} yr^{-1}] is the reaction rate, dt_{num} is the time step used in the specific model run, and $SC_{s,d}$ is a stoichiometric factor. The maximum rates are used as long as they can be fulfilled by the available amount of the reactant. If the amount decreases, the rates were automatically reduced to avoid negative concentrations [36]. Sulfate bottom water concentration of 28 mmol L^{-1} and methane concentration of 0.0 mmol L^{-1}, as the major pore water parameters, were defined as the upper boundary condition. To allow diffusion across the boundary, the lower boundary is defined as an open/transmissive boundary. The diffusive flux of methane into the model area from below was defined by using a fixed methane concentration. This methane value was defined to create the gradient necessary to simulate the measured influx of CH_4. All input parameters are given in the respective section below.

3. Results and discussion

3.1. Authigenic barite fronts

In contrast to the non-reactive terrigenous Ba phase, biogenic barium is discussed as the labile Ba phase which is subject to (partial) remobilization in marine sediments due to sulfate depletion (e.g. [22,38]). The biogenic barium fraction is part of excess barium that can be calculated from the total amount of solid phase barium and the ratio of terrigenous Ba/Al or Ba/Ti [4,39,40] or determined by sequential extraction [14,41]. At high productivity area, the main amount of excess Ba in the underlying sediments is composed of barite [42]. Because of the high productivity within the Benguela upwelling area the input of reactive (biogenic) barium into the sediment in this area is high, while the amount of terrigenous barium is low [40,43].

The pore water and solid phase barium profiles at site GeoB 8426 (Fig. 2) display the typical diagenetic cycling of barium as discussed by von Breymann et al. [9]. The reactive solid phase barium is dissolved in the sulfate-depleted zone below the SMT and Ba^{2+} is released into the pore water:

$$Ba^{2+} + SO_4^{2-} \leftrightarrow BaSO_4 \quad (2)$$

The upward migration of the dissolved barium into the sulfate-bearing zone leads to the precipitation of authigenic barite at the SMT which is currently located at about 3.20 mbsf at site GeoB 8426. Just below the SMT, the solid phase profile shows a pronounced Ba peak (Fig. 2). This Ba enrichment contains barite par-

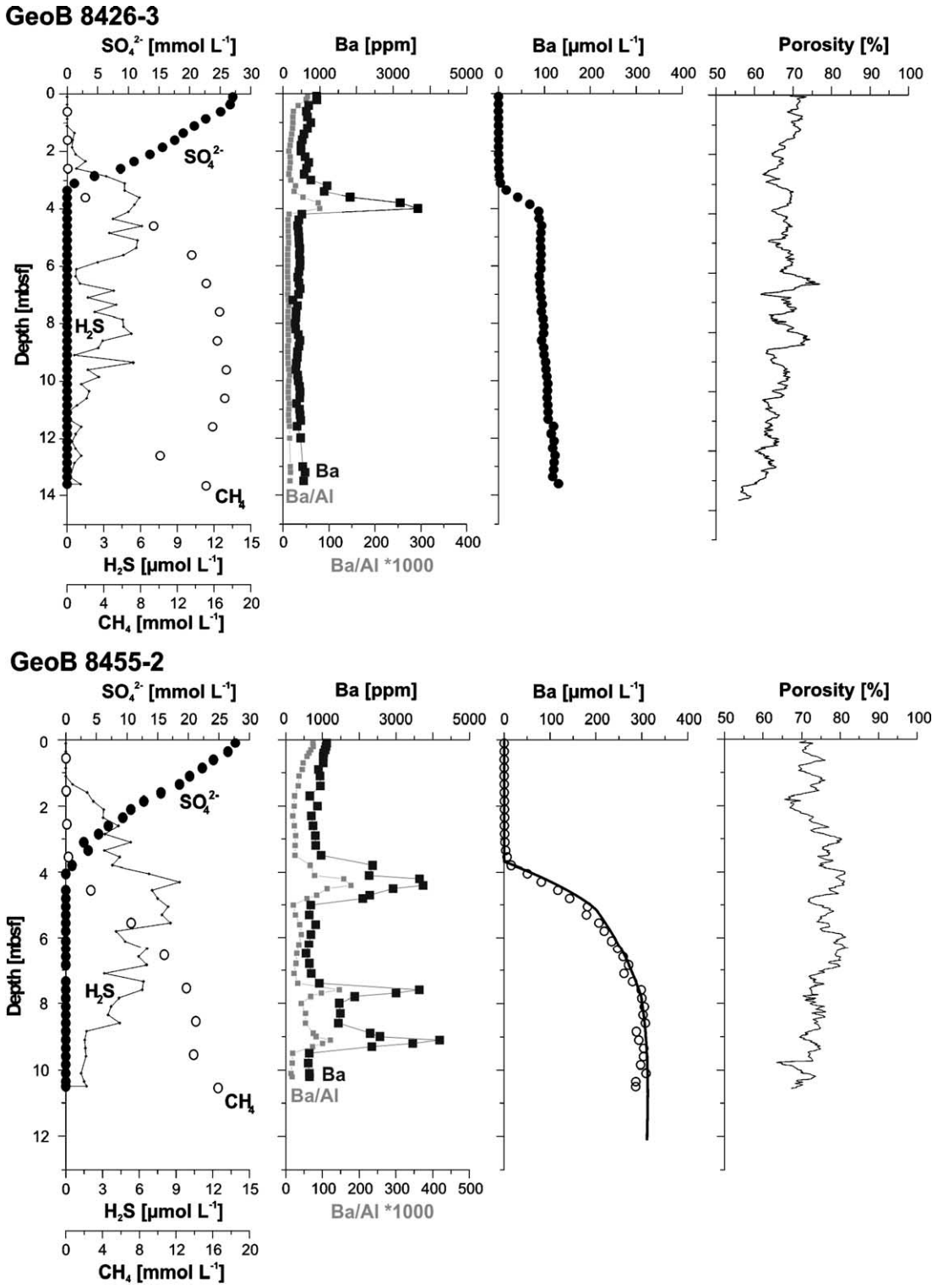

Fig. 2. Profiles of pore water and solid phase at sites GeoB 8426 and GeoB 8455. At both sites barium enrichments occur with a second small peak at the current sulfate/methane transition (SMT). At site GeoB 8455 two further barium enrichments are located a few meters below the SMT, indicating a release of barium into the pore water displayed by the dissolved barium profile. The solid line indicates the modeled pore water profile of barium.

ticles which partially show dissolution structures (Fig. 3A). The "double" barium peak indicates a recent upward shift in the SMT, with the small uppermost peak representing the site of the current/active barite front. Due to the diagenetic cycling of reactive barium, the authigenic barite peak is slowly but constantly growing. The active front slowly moves upward, keeping a constant offset to the sediment surface, corresponding to the SMT.

The penetration depth of sulfate in the study area is controlled by the anaerobic oxidation of methane (AOM) as shown by Niewöhner et al. [44]. At the SMT sulfate is consumed, and hydrogen sulfide is produced due to AOM (e.g. [45,46]):

$$CH_4 + SO_4^{2-} \rightarrow HCO_3^- + H_2O + HS^- \quad (3)$$

The sulfate pore water profiles of the investigated cores GeoB 8426-3 and GeoB 8455-2 show linear decrease with depth (Fig. 2). At site GeoB 8455 the SMT is located at about 3.80 mbsf, where solid phase barium is enriched similar to site GeoB 8426 with a second larger peak slightly below the SMT. In contrast to site GeoB 8426, the barium solid phase profile at site GeoB 8455 is characterized by the occurrence of two further distinct Ba-peaks a few meters below the SMT (Fig. 2). The shape of the barium pore water profile reveals that the deeper buried barium enrichments provide a source of barium to the pore water. This indicates the presence of reactive Ba solid phase. Selected representative samples analyzed by SEM and EDS indicate that the main Ba mineral present in the barium solid phase is barite. Although the deeper buried barite fronts, at depths of about 7.69 and 9.18 mbsf, are dominated by rather small particles, the shape of the barite crystals is similar to those found within the barite peak at the SMT. Some barite crystals from the barite fronts in the sediments of core GeoB 8455-2 are displayed in Fig. 3C–H. In contrast to the displayed barite particles at 4.22 mbsf, the barite grains at 7.69 and 9.18 mbsf show strong dissolution structures.

3.2. Time calculations for the formation of barite enrichments

Under the premise of a constant diffusive upward flux of barium into the sulfate-bearing zone, we calculated the time needed to produce the measured barium enrichment in the solid phase at the SMT. The duration of barium precipitation can be simulated assuming linear diffusive concentration gradients over time (cf. [17]). Similar calculations for the enrichment of iron sulfides were carried out by Kasten et al. [47]. Slight changes in the average porosity have substantial influence on the calculated enrichment periods. It has to be clearly pointed out that the calculated time needed for the formation of each barium enrichment is just an approximation due to these uncertainties. The calculation of the diffusive fluxes was performed according to Fick's first law with a diffusion coefficient in free solution (D_0) for barium of 147.6 $cm^2\ yr^{-1}$ which was corrected for tortuosity [37]. The refractory amount of solid phase barium (the mean concentration of barium in the lowermost core sediments) at sites GeoB 8426 and GeoB 8455 amounts to 500 and 650 ppm, respectively, and the dry density of the bulk sediment averages 2.7 $g\ cm^{-3}$. If we assume an average porosity of 70% for sediments at site GeoB 8426 and 75% for site GeoB 8455, the time needed to produce the observed barium peaks at the SMT would be about 14,000 yr. The variation of the enrichment period due to different porosities is given in Table 2. Assuming a decreasing barium flux with time due to the decreased amount of reactive barite at the deeper buried barium fronts or a decreased dissolution rate, the calculated times would be slightly overestimated. However, the results of the calculation emphasize that the barite enrichments in the deeper sediments at site GeoB 8455 were exposed to a sulfate-depleted environment for at least ten thousand years.

3.3. Numerical modeling

To assess the influence of different mechanisms and/or conditions (e.g. dissolution rates, diffusive barium fluxes, or variations in methane flux or sedimentation rate) on the amount and depth of solid phase barium, we simulated different scenarios by numerical modeling using the transport and reaction model CoTReM.

Dissolution rates for core GeoB 8455-2 were modeled by simulating the measured pore water profile of barium. This computer simulation is based on the assumption that the amount of diagenetic barite which precipitated at the SMT, was primarily supplied by upward diffusion of dissolved barium, resulting from the dissolution of labile barite in the sediment buried below the SMT, and the recycling of input barite at the SMT. The concen-

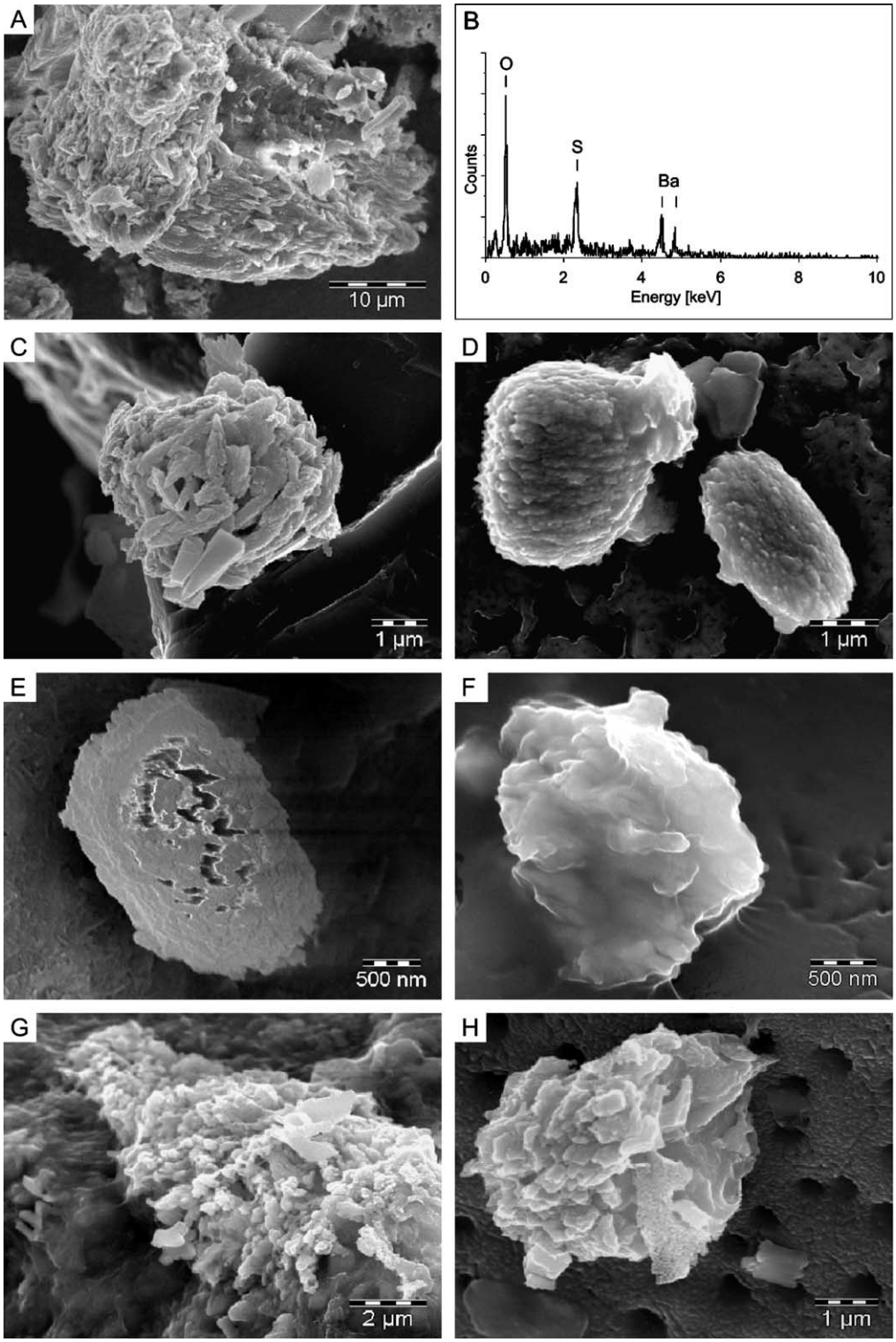

Fig. 3. Scanning electron microscope images of barite crystals. (A) Large barite particle at site GeoB 8426 slightly below the SMT (3.83 mbsf). (B) Energy dispersive spectra (EDS) of the barite particles displayed in (D). Images of barite at site GeoB 8455 at: (C) and (D): 4.22 mbsf. (E) and (F): 7.69 mbsf. (G) and (H): 9.18 mbsf. The barite particles of the last four panels (E–H) show strong dissolution structures.

Table 2
Calculation of the time needed for the formation of barite enrichment at the SMT for different porosities

Core	Ba gradient [mol m^{-3} cm^{-1}]	Porosity [%]	Period of time [yr]
GeoB 8426-3	9.424 10^{-10}	65	19,905
		70	14,581
		75	10,428
GeoB 8455-2	1.330 10^{-09}	70	19,170
		75	13,709
		80	9439

The Ba flux is assumed to be constant over time, and the sediment dry density averages 2.7 g cm^{-3} .

tration of refractory solid phase barium below the SMT was set to 650 ppm and the mean measured input concentration above the SMT was 1000 ppm. Methane concentration at the lower boundary was set to 36 mmol/L transferred from the current gradient into the zone of SMT. For site GeoB 8455 the porosity of the sediment averages 75% (Fig. 2) and we used a mean sedimentation rate of 10 cm kyr^{-1}, adopted from adjacent sampling sites at similar water depths with sedimentation rates of 8–11 cm kyr^{-1} [48,49].

Modeling of the measured barium pore water profile of site GeoB 8455 (Fig. 2) reveals that the dissolution rate of barite directly below the SMT is higher than at the deeper buried Ba enrichments with rates of 1.1 μmol dm^{-3} yr^{-1}. This rate is similar to the dissolution rate for barite dissolution at methane cold seeps reported by Aloisi et al. [50]. The modeled dissolution rate decreases with depth down to 0.05 μmol dm^{-3} yr^{-1}. This indicates that the dissolution of barite at these deeper fronts is retarded compared to the dissolution rates directly below the SMT. A further interesting outcome of the model is that at steady-state conditions the shape of the barium peak at the SMT (mainly) depends on dissolution rate and sedimentation rate.

At the investigated sites, barite enrichments at the SMT are characterized by a large peak and a second, smaller one on top, representing the current barite front. Thus, there must have been a slight recent upward shift of the SMT, resulting in the formation of the uppermost barite enrichment. To find out whether this process is limited to the investigated sites, we compared barium solid phase data of adjacent coring sites GeoB 3703 and GeoB 3718 (Fig. 4). The occurrence of similar barium profiles with a second larger

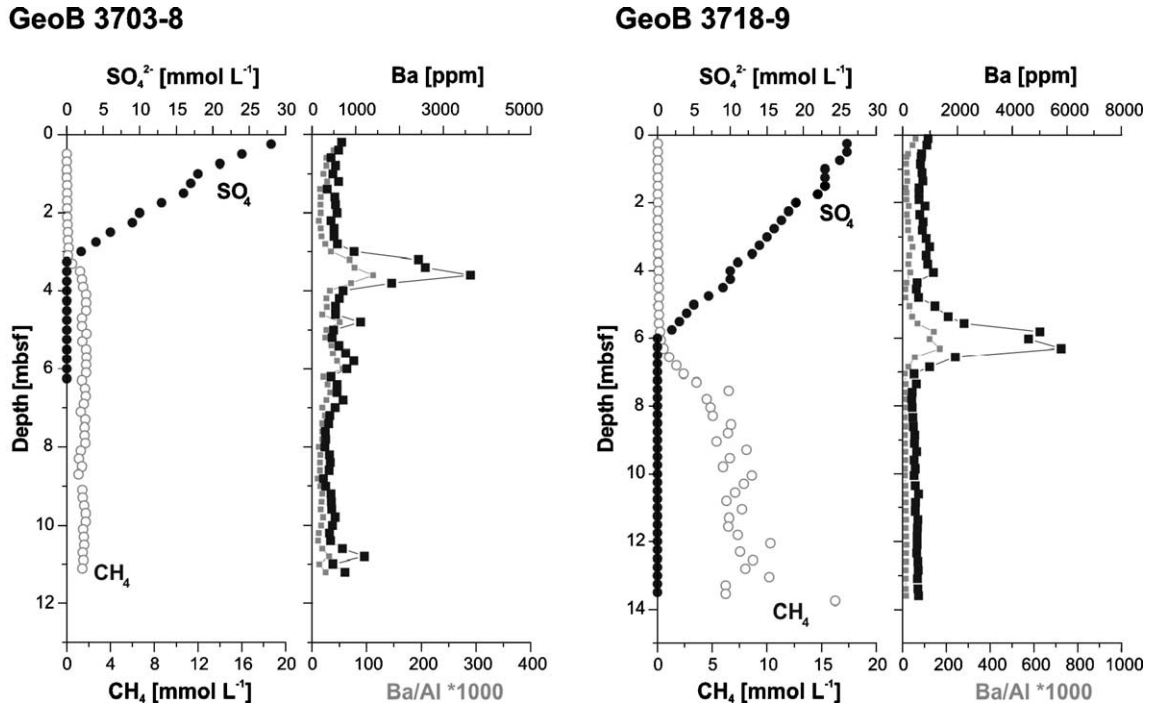

Fig. 4. Pore water and solid phase profiles at sites GeoB 3703 and GeoB 3718. At the current SMT a second smaller peak occurs at both sites. The pore water data of sulfate and methane are taken from Niewöhner et al. [44]. Solid phase data of core GeoB 3718-9 according to Kasten et al. [47].

peak directly below the SMT at all investigated stations reveal that the formation of these enrichments is influenced by more regional process.

Modeling the current positions of the barium peaks in core GeoB 8455-2 indicates enrichment due to nonsteady-state situations. At steady-state conditions only a single barite peak can be modeled. Increasing sedimentation rate or methane flux leads to the formation of a second barite peak. Possible nonsteady-state processes causing the formation of the observed barite fronts could be related to the sediment composition, the depositional dynamics, such as drastic changes in the sedimentation rate, or variations in the upward methane flux. An increase in the upward flux of methane over a larger area can be caused by the degradation of organic matter in deeper sediments, or the decomposition of gas hydrate. High resolution echosounder profiles, as recorded by the PARASOUND shipboard system during the cruises, indicate no depositional irregularities (e.g. caused by gravity mass flows). This is in good agreement with results from previous studies for this area [27]. Thus, the shift of the SMT cannot be explained by such depositional dynamics.

Although the thermodynamic stability criteria for gas hydrate at the sampling sites are fulfilled, chemical indications of their existence were not found in the sediment. An increase in methane concentrations could be also explained by the burial of high amounts of non-refractive organic matter below the SMT and the resulting elevated rates of methanogenesis due to the degradation of the organic matter. This process is likely regional. Regional processes can only account for the recent shift of the SMT leading to the formation of the small current barite peak which was found at both studied sites. In contrast, the finding of additional barium enrichments below the SMT is limited to site GeoB 8455. However, because the sedimentary records do not indicate any sedimentary event (e.g. slumps, slides), we assume that a change in the methane flux is the only process which also explains the prior pronounced shift in the SMT, and thus the preservation of additional barium fronts a few meters below the current SMT.

3.4. Barite enrichments below the SMT

In sulfate-depleted marine sediments, barite is supposed to be unstable. The occurrence of barite enrichments below the SMT at site GeoB 8455 indicates that there are processes or conditions increasing the stability of barite in the sulfate-depleted sediments. One mechanism in this regard could be the strikingly high amount of total barium in the sediment system at site GeoB 8455 (Fig. 2). High concentrations of dissolved barium below the SMT could influence the dissolution rate of barite. Modeling pore water data from site GeoB 8455 at 7.6 mbsf by using PHREEQC 2.10 [51] indicates that for an initial barium concentration of 300 μmol L^{-1} a low sulfate concentration of about 5 μmol L^{-1} would be sufficient to obtain barite saturation (with an equilibrium constant (log KT) of −10.40 at a temperature of 3 °C).

However, sediment volume-normalised dissolution rates are dependent both on the saturation state of fluids and on the concentration of $BaSO_4$ in sediments. Thus, the decrease of the barite dissolution rate with depth that we calculate with the model may be due to changes in the concentration of barite in the sediment, as well as changes in the saturation state of fluids.

Another explanation for the enrichment of barium minerals in the sulfate-depleted zone could be the occurrence of other Ba phases that show oxygen depletion relative to barite. Energy dispersive spectra of barium particles from the deeper buried barium enrichments at site GeoB 8455 reveal that some barium phases have low oxygen concentrations while the amount of sulfur and barium is constant and only the carbon concentration increases (Fig. 5). This suggests that some barite particles were altered, or that primary sulfate-free Ba phases exist. González-Muñoz et al. [52] reported microbially mediated precipitation of barite under laboratory conditions, and found that Ba phases were incorporated into spherical aggregates without sulfate. These spherical aggregates of 0.5 to 1 μm in diameter show a striking similarity to some of the barium particles which are found within the barium enrichments at site GeoB 8455 (Fig. 5C). The observed spherical aggregates described by González-Muñoz et al. [52] mainly contained barium and phosphorus and were supposed to represent an early stage of crystal growth. This does not necessarily imply that the spherical aggregates found in core GeoB 8455-2 were formed by bacterially mediated processes, but that the crystals either are in an early stage of growth or that the growth of the crystals was inhibited at an early stage.

Another process which could explain the occurrence of oxygen-depleted barium phases compared to barite, would be the dissimilatory reduction of sulfate from barite, as investigated by Baldi et al. [53]. Based on laboratory results they discussed the microbial reduc-

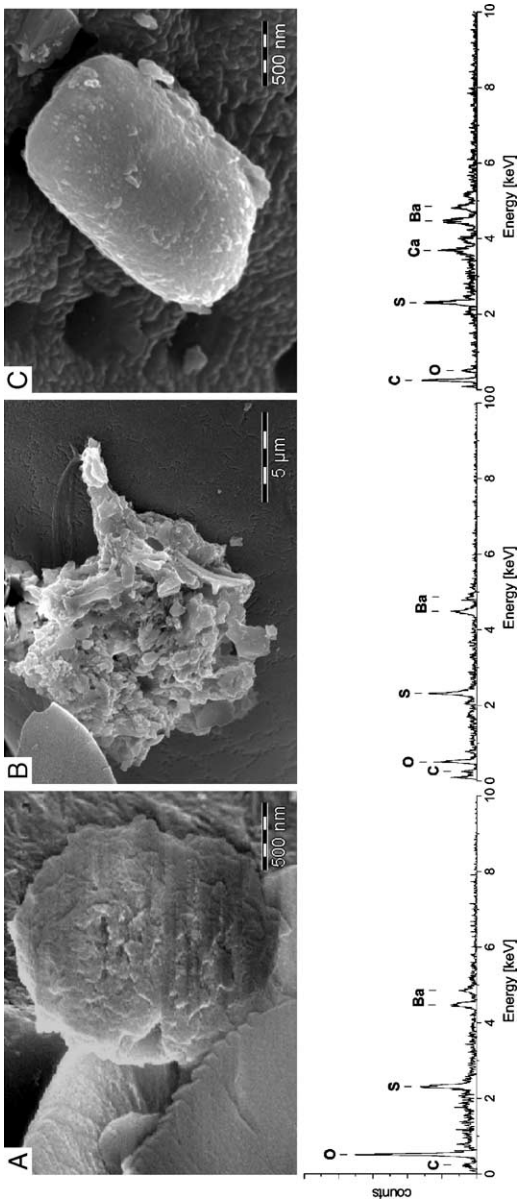

Fig. 5. At site GeoB 8455. (A) Barite crystal at 7.69 mbsf with a characteristic barite ratio of barium, sulfur, and oxygen. (B) Larger barite crystal with strong dissolution structures at 9.18 msbf. The EDS spectrum indicates a decreased oxygen concentration. (C) Barium particle at 9.18 mbsf with calcium incorporations and carbon, but low oxygen concentrations.

tion of barite via the formation of other barium compounds, such as witherite ($BaCO_3$) and the transient species barium sulfide (BaS). These coexisting barium phases were also reported by Malysh et al. [54]. They examined the influence of carbon-containing phases on the reduction of recycled barite in laboratory experiments. The reduction of barite or more precisely the reduction of barium-sulfate, with carbon leads to the formation of witherite via the transient phase barium sulfide:

$$BaSO_4 + 2C \rightarrow BaS + 2CO_2 \quad (4)$$

$$BaS + CO_2 + H_2O \rightarrow BaCO_3 + H_2S \quad (5)$$

This process is accelerated due to the catalyzing effect of the formed barium sulfide particles [54]. Furthermore, the conversion of barite into barium sulfide could lead to a sulfide coating, which can be compared with coatings of ferric iron minerals by iron sulfides in sulfidic sediments (e.g. [55]). This process could shield the barite particle, covered with barium sulfide, from further dissolution. It would also provide a small sink for hydrogen sulfide in deeper sediments. One indication for the process of barite reduction to occur in this environment is the increasing amount of carbon with decreasing oxygen concentrations found in some of the barium particles from the deeper buried barite fronts at site GeoB 8455 (Fig. 5). The sediments of the coring sites are characterized by high concentrations of hydrogen sulfide, high alkalinity (up to 80 mmol(eq) L^{-1}), and high amounts of TOC, and thus would provide a suitable environment for the alteration of barite into witherite (via barium sulfide). However, these processes in marine sediments require further investigations.

4. Conclusions

Sediments of two sites from the Eastern Cape Basin were examined for pore water and solid phase geochemistry. Small uppermost barium enrichments at both sites at the current SMT and large barium peaks slightly below imply a small upward shift of the SMT in the recent past which is likely to be a widespread regional phenomenon in the study area. At one site, distinct solid phase barium enrichments occur a few meters below the SMT in sulfate-depleted sediments which are dominated by small barite particles. These preserved buried barite fronts indicate former positions of the SMT. We assume that the abrupt relocation of the SMT, and thus the formation of

new barite fronts, is most likely triggered by an increase in the upward flux of methane. Calculations of the formation time of these enrichments and numerical modeling suggest that this shift of the SMT occurred between the last glacial maximum (LGM) and the Pleistocene/Holocene transition. High amounts of non-refractive organic matter buried below the SMT which lead to higher rates of methanogenesis, could explain such increases in methane concentrations and fluxes. Furthermore, the detection of barite below the SMT indicates that although being metastable/unstable in the prevailing geochemical environments, such minerals can be preserved/shielded from dissolution by specific processes or mechanisms, and thus be buried into deeper sediments. At such depths barite, for example, could fuel/support AOM to proceed below the SMT. Thus, reactive minerals buried in deeper sediments can have great influence on biogeochemical processes in the deep biosphere by providing terminal electron acceptors.

Acknowledgements

We thank the crew and scientists aboard the RV *Meteor* for their strong support during cruises M34/2 and M57/2. For technical assistance on board and in the home laboratory we are indebted to S. Hessler, S. Hinrichs, and S. Siemer. SEM analyses were carried out at Utrecht University, EMSA. The people there are thanked for their hospitality and cooperation. G. Aloisi, G. Bohrmann, M. Kölling, and M. Zabel are thanked for detailed comments on an earlier version of the manuscript. We thank J. Nüster for reading an earlier draft of this manuscript. Our special appreciation goes to C. Hensen and H.D. Schulz for helpful discussions. The manuscript greatly benefited from detailed comments and corrections of two anonymous reviewers. This research was funded by the Deutsche Forschungsgemeinschaft as part of the Research Center "Ocean Margins" (RCOM) of the University of Bremen, contribution no. RCOM0343.

References

[1] E.D. Goldberg, G.O.S. Arrhenius, Chemistry of Pacific pelagic sediments, Geochim. Cosmochim. Acta 13 (1958) 153–212.
[2] T.M. Church, Marine Barite, in: R.G. Burns (Ed.), Marine Minerals, Rev. Mineral., Miner. Soc. Am., vol. 6, 1979, pp. 175–209.
[3] J.K. Bishop, The barite–opal–organic carbon association in oceanic particular matter, Nature 24 (1988) 341–343.
[4] J. Dymond, E. Suess, M. Lyle, Barium in deep-sea sediment: a geochemical proxy for paleoproductivity, Paleoceanography 7 (1992) 163–181.
[5] T.J. Chow, E.D. Goldberg, On the marine geochemistry of barium, Geochim. Cosmochim. Acta 20 (1960) 192–198.
[6] F. Dehairs, R. Chesselet, J. Jedwab, Discrete suspended particles of barite and the barium cycle in the open ocean, Earth Planet. Sci. Lett. 49 (1980) 915–931.
[7] F. Dehairs, N. Stroobants, L. Goeyens, Suspended barite as a tracer of biological activity in the Southern Ocean, Mar. Chem. 35 (1991) 399–410.
[8] R.S. Ganeshram, R. Franc, J. Commeau, S.L. Brown-Leger, An experimental investigation of barite formation in seawater, Geochim. Cosmochim. Acta 67 (2003) 2599–2605.
[9] M.T. von Breymann, H. Brumsack, K.-C. Emeis, Depositional and diagenetic behavior of barium in the Japan Sea, in: K.A. Pisciotto, J.C. Ingle, M.T. von Breymann, J. Barron, et al., (Eds.), Proc. ODP, Sci. Resul. 127/128, College Station, Texas, USA, 1992, pp. 651–663.
[10] F. Gingele, A. Dahmke, Discrete barite particles and barium as tracers of paleoproductivity in South Atlantic sediments, Paleoceanography 9 (1994) 151–168.
[11] A. Paytan, M. Kastner, F.P. Chavez, Glacial to interglacial fluctuations in productivity in the Equatorial Pacific as indicated by marine barite, Science 274 (1996) 1355–1357.
[12] F.X. Gingele, M. Zabel, S. Kasten, W.J. Bonn, C.C. Nürnberg, Biogenic barium as a proxy for paleoproductivity: methods and limitations of application, in: G. Fischer, G. Wefer (Eds.), Use of Proxies in Paleoceanography: Examples from the South Atlantic, Springer, 1999, pp. 345–364.
[13] S. Mearon, A. Paytan, T.J. Bralower, Cretaceous strontium isotope stratigraphy using marine barite, Geology 31 (2002) 15–18.
[14] A. Paytan, M. Kastner, E.E. Martin, J.D. Macdougall, T. Herbert, Marine barites as a monitor of seawater strontium isotope composition, Nature 366 (1993) 445–449.
[15] G.R. Dickens, Sulfate profiles and barium fronts in sediment on the Blake Ridge: present and past methane fluxes through a large gas hydrate reservoir, Geochim. Cosmochim. Acta 65 (2001) 529–543.
[16] A. Paytan, M. Kastner, D. Campbell, M.H. Thiemens, Sulfur isotope composition of Cenozoic seawater sulfate, Science 282 (1998) 1459–1462.
[17] A. Paytan, M. Kastner, D. Campbell, M.H. Thiemens, Seawater sulfur isotope fluctuations in the cretaceous, Science 304 (2004) 1663–1665.
[18] J. McManus, W.M. Berelson, G.P. Klinkhammer, K.S. Johnson, K.H. Coale, R.F. Anderson, N. Kumar, D.J. Burdige, D.E. Hammond, H.J. Brumsack, D.C. Mccorkle, A. Rushdi, Geochemistry of barium in marine sediments: implications for its use as a paleoproxy, Geochim. Cosmochim. Acta 62 (1998) 3453–3473.
[19] A. Paytan, S. Mearon, K. Cobb, M. Kastner, Origin of marine barite deposits: Sr and S isotope characterization, Geology 30 (2002) 747–750.
[20] D.S. Cronan, Authigenic minerals in deep-sea sediments, in: E.D. Goldberg (Ed.), The Sea, vol. 5, Wiley Interscience, 1974, pp. 491–525.
[21] W.E. Dean, B.C. Schreiber, Authigenic barite, leg 41 deep sea drilling project, in: Y. Lancelot, E. Seibold, et al., (Eds.), Proc. ODP, Init. Repts., vol. 41, U.S. Gov. Off., Washington, D.C., 1978, pp. 915–931.
[22] M.E. Torres, H.J. Brumsack, G. Bohrmann, K.C. Emeis, Barite fronts in continental margin sediments: a new look at barium remobilization in the zone of sulfate reduction and formation of

heavy barites in diagenetic fronts, Chem. Geol. 127 (1996) 125–139.
[23] S. Kasten, B.B. Jørgensen, Sulfate reduction in marine sediments, in: H.D. Schulz, M. Zabel (Eds.), Marine Geochemistry, Springer, 2000, pp. 263–281.
[24] S. Kasten, M. Zabel, V. Heuer, C. Hensen, Processes and signals of nonsteady-state diagenesis in deep-sea sediments and their pore waters, in: G. Wefer, S. Mulitza, V. Ratmeyer (Eds.), The South Atlantic in the Late Quaternary: Reconstruction of Material Budget and Current Systems, Springer, 2003, pp. 431–459.
[25] S.P. Varnavas, Marine barite in sediments from deep sea drilling project sites 424 and 424A (Galapagos hydrothermal mounds field), Mar. Chem. 20 (1987) 245–253.
[26] M.E. Torres, G. Bohrmann, E. Suess, Authigenic barites and fluxes of barium associated with fluid seeps in the Peru subduction zone, Earth Planet. Sci. Lett. 144 (1996) 469–481.
[27] R.W. Embley, J.J. Morley, Quaternary sedimentation and paleoenvironmental studies off Namibia (South-West Africa), Mar. Geol. 36 (1980) 183–204.
[28] L.V. Shannon, The Benguela ecosystem: Part 1. Evolution of the Benguela, physical features and processes, Oceanogr. Mar. Biol. Annu. Rev. 23 (1985) 105–182.
[29] G. Wefer, G. Fischer, Seasonal patterns of vertical flux in equatorial and coastal upwelling areas of the eastern Atlantic, Deep-Sea Res. I 40 (1993) 1613–1645.
[30] L.V. Shannon, G. Nelson, The Benguela: large scale features and processes and system variability, in: G. Wefer, W. Berger, G. Siedler, D. Webb (Eds.), The South Atlantic: Present and Past Circulation, Springer, 1996, pp. 163–210.
[31] J.M. Bremner, J.P. Willis, Mineralogy and geochemistry of the clay fraction of sediments from the Namibian continental margin and the adjacent hinterland, Mar. Geol. 115 (1993) 85–116.
[32] J. Rogers, J.M. Bremner, The Benguela ecosystem: Part VII. Marine-geological aspects, Oceanogr. Mar. Biol. Annu. Rev. 29 (1991) 1–85.
[33] C.P. Summerhayes, B.D. Bornhold, R.W. Embley, Surficial slides and slumps on the continental slope and rise off South-West Africa, Mar. Geol. 31 (1979) 265–277.
[34] H.D. Schulz, Quantification of early diagenesis: dissolved constituents in marine pore water, in: H.D. Schulz, M. Zabel (Eds.), Marine Geochemistry, Springer, 2000, pp. 85–128.
[35] M. Adler, C. Hensen, H.D. Schulz, CoTReM-Column Transport and Reaction Model. http://www.geochemie.uni-bremen.de/downloads/cotrem/index.htm, User Guide, Version 2.3 (2000).
[36] M. Adler, C. Hensen, F. Wenzhöfer, K. Pfeifer, H.D. Schulz, Modeling of subsurface calcite dissolution by oxic respiration in supralysoclinal deep-sea sediments, Mar. Geol. 177 (2001) 167–189.
[37] B.P. Boudreau, Diagenetic Models and Their Implementation: Modeling Transport and Reactions in Aquatic Sediments, Springer, 1997.
[38] J. McManus, W.M. Berelson, G.P. Klinkhammer, T.E. Kilgore, D.E. Hammond, Remobilization of barium in continental margin sediments, Geochim. Cosmochim. Acta 58 (1994) 4899–4907.
[39] K.B. Averyt, A. Paytan, A comparison of multiple proxies for export production in the equatorial Pacific, Paleoceanography 19 (2004) , doi:10.1029/2004PA001005.
[40] A. Reitz, K. Pfeifer, G.J. de Lange, J. Klump, Biogenic barium and the detrital Ba/Al ratio: a comparison of their direct and indirect determination, Mar. Geol. 204 (2004) 289–300.
[41] A. Rutten, G.J. de Lange, A novel selective extraction of barite, and its application to eastern Mediterranean sediments, Earth Planet. Sci. Lett. 198 (2002) 11–24.
[42] M. Eagle, A. Paytan, K.R. Arrigo, G. van Dijken, R.W. Murray, A comparison between excess barium and barite as indicators of carbon export, Paleoceanography 18 (2003) 21–1–21–13.
[43] K. Pfeifer, S. Kasten, C. Hensen, H.D. Schulz, Reconstruction of primary productivity from the barium contents in surface sediments of the Atlantic Ocean, Mar. Geol. 177 (2001) 13–27.
[44] C. Niewöhner, C. Hensen, S. Kasten, M. Zabel, H.D. Schulz, Deep sulfate reduction completely mediated by anaerobic methane oxidation in sediments of the upwelling area off Namibia, Geochim. Cosmochim. Acta 62 (1998) 455–464.
[45] R.O. Barnes, E.D. Goldberg, Methane production and consumption in anoxic marine sediments, Geology 4 (1976) 297–300.
[46] B.B. Bernard, Methane in marine sediments, Deep-Sea Res. 26A (1979) 429–443.
[47] S. Kasten, T. Freudenthal, F.X. Gingele, H.D. Schulz, Simultaneous formation of iron-rich layers at different redox boundaries in sediments of the Amazon deep-sea fan, Geochim. Cosmochim. Acta 62 (1998) 2253–2264.
[48] B. Donner, M. Giese, Stratigraphie und Smear-Slide-Analysen, in: D. Schulz, cruise participants (Eds.), Berichte und erste Ergebnisse über die Meteor-Fahrt M20/2, Abidjan - Dakar, 27.12.1991–2.2.1992, Ber. Fachb. Geowiss. Univ. Bremen, vol. 25, 1992, pp. 51–80.
[49] G. Mollenhauer, R.R. Schneider, P.J. Müller, V. Spieβ, G. Wefer, Glacial/interglacial variability in the Benguela upwelling system: spatial distribution and budgets of organic carbon accumulation, Glob. Biogeochem. Cycles 16 (2002) 1134.
[50] G. Alosi, K. Wallmann, S.M. Bollwerk, A. Derkachev, G. Bohrmann, E. Suess, The effect of dissolved barium on biogeochemical processes at cold seeps, Geochim. Cosmochim. Acta 68 (2004) 1735–1748.
[51] D.L. Parkhurst, C.A.J. Appelo, User's guide to PHREEQC (Version 2.0), U.S. Geol. Surv., Water Resour. Inv. Rep., 1999, pp. 99–4259.
[52] M.T. Gonzáles-Muñoz, B. Fernández-Luque, F. Martínez-Ruiz, K.B. Cheroun, J.M. Arias, M. Rodríguez-Gallego, M. Martínez-Cañamero, C. de Linares, A. Paytan, Precipitation of barite by *Myxococcus xanthus*: possible implications for the biogeochemical cycle of barium, Appl. Environ. Microbiol. 69 (2003) 5722–5725.
[53] F. Baldi, M. Pepi, D. Burrini, G. Kniewald, D. Scali, E. Lanciotti, Dissolution of barium from barite in sewage sludges and cultures of *Desulfovibrio desulfuricans*, Appl. Environ. Microbiol. 62 (1996) 2398–2404.
[54] L.A. Malysh, L.G. Gaisin, M.F. Volkova, A.G. Prokhorov, K.V. Tkachev, Reduction of recycled barium sulfate, Russ. J. Appl. Chem. 75 (2002) 14–17.
[55] J.F.L. Garming, U. Bleil, N. Riedinger, Alteration of magnetic mineralogy at the sulfate methane transition: analysis of sediments from the Argentine continental slope, Phys. Earth Planet. Inter. 151 (2005) 290–308.